Hadronization of a quark-gluon plasma in the chromodielectric model

C. T. Traxler and U. Mosel
Institut für Theoretische Physik, Universität Giessen, D-35392 Giessen, Germany

T. S. Biró
Research Institute for Particle and Nuclear Physics, Budapest, H-1525 Budapest, Hungary

(Received 11 August 1998)

We have carried out simulations of the hadronization of a hot, ideal but effectively massive quark-gluon gas into color-neutral clusters in the framework of the semiclassical SU(3) chromodielectric model. We have studied the possible quark-gluon compositions of clusters as well as the final mass distribution and spectra, aiming to obtain insight into relations between hadronic spectral properties and the confinement mechanism in this model. [S0556-2813(99)04303-4]

PACS number(s): 12.38.Mh, 12.38.Lg, 24.85.+p

I. INTRODUCTION

The quest for the quark-gluon plasma (QGP) is one of the major scientific efforts of the last decade of strong interaction physics. In recent years 200*A* GeV Pb beams became available for experimental study at CERN SPS, and future colliders will reach even higher energies, namely, (200 +200)*A* GeV at RHIC Brookhaven and (6300+6300)*A* GeV at CERN LHC. These energies correspond to an estimated maximal energy density of $\varepsilon = 5$ GeV/fm^3 and $\varepsilon = 9$ GeV/fm^3 or temperature $T = 230$ MeV and $T = 260$ MeV, respectively. At CERN SPS the achieved maximal temperature is about $T = 160$ MeV [1].

Heavy ions like Au and Pb are the best means for approaching the thermodynamical limit in particle accelerator experiments as closely as possible. They provide high energy and baryon densities. These advantages on the experimental side lead to trouble for theoretical studies: although the thermodynamical approach to quark matter is highly developed [2,3], dynamical and finite baryon density studies are at their very beginning [4,5]. The solution of both theoretical problems, i.e., a real-time description and study at finite density, is connected to the invention of new nonperturbative techniques, which are able to handle complex effective actions. On the other hand, there are several phenomenological models aiming to simulate these unknown dynamical features of quantum chromodynamics (QCD).

In theoretical works the main goal is to understand the mechanism of *color confinement*. In this perspective, understanding hadronization means learning about the confinement mechanism in an experimentally controllable situation. We briefly review hadronization models presently known to us grouped in three categories: *prompt, equilibrium*, and *evolutionary*. The process takes zero (i.e., less than 1 fm/c), an infinite (more than 20 fm/c), or a finite (2–6 fm/c) amount of time in these three respective categories.

String- and parton-fragmentation models [6,7] in the first category are the oldest prompt hadronization models; they have been used already in the description of elementary particle collisions (pp, $p\bar{p}$, and e^+e^-). With the help of Glauber's model [8] the yields of elementary pp events are then summed up for a complicated heavy ion collision. In these calculations hadron ratios depend on phenomenological fragmentation ratios or fragmentation functions [9]. Although these parameters are nonperturbative, any explanation or derivation of them from QCD is missing.

Further statistical and combinatorical models connect quark numbers and (pre)hadron numbers by assuming an underlying coalescence. The quark cluster model used, e.g., in the parton cascade model [10] or partially in string models like VENUS [11] and (U)RQMD [12] is sensitive to quark properties, like effective masses. The ALCOR model [13] assumes an extremely fast and far-from-equilibrium hadronization of massive quarks after gluons are fragmented. Although individual hadron formation is immediate, the formation time instant may vary over a range of several tens of fm/c in these approaches. In these models hadron formation is a process, whose explanation is still absent.

In contrast, the mixed phase model [14]—one of the most recent representatives of the second category—focuses on the state of thermodynamical equilibrium. It constructs a nonideal equation of state which includes part of the particle correlations and is able to show confinement behavior. Although—in our opinion—this is a promising research direction, it fails to describe a very nonequilibrium hadronization, where the characteristic time of bound quark cluster formation is commensurate with the thermal equilibrium maintenance time. Also, diquarks and baryons have not been included yet.

There are several chemical approaches to hadronization, showing an evolution time of a few to several fm/c. Assuming a massive, effectively nonrelativistic quark matter, the hadronization can be described by utilizing phenomenological confinement potentials or just the perturbative Coulomb-like potential. The elimination of color charge during this process is then due to medium effects, like string formation. The time evolution of the mixed quark-hadron system is described by a set of rate equations. Such an approach was published a decade ago [15], and is recently under development in the framework of the ALCOR model [16].

Also in the framework of Nambu–Jona-Lasinio (NJL) model hadronization cross sections have been obtained [17]. Since mesons, like pions and σ mesons, are elementary in

this model, the confinement mechanism, an important detail of the microscopic process, remains unexplored. An alternative model, the chromodielectric model (CDM) originally proposed by Friedberg and Lee [18], describes hadrons as clusters of quarks bound in a phenomenological scalar potential. While there have been a tantamount number of studies of stationary states of this model with quantum-mechanical quarks [19–22], a real-time dynamical approach is quite recent [23–26]. The latter studies utilized semiclassical transport theory, treating quarks like classical charge clouds.

In the present paper we report on a classical molecular dynamics approach on the quark level to hadronization. For the dynamical description, the classical limit of the CDM is used, where quarks and gluons are represented by extended but rigid charge distributions. The background fields are a scalar field and two Abelian fields, corresponding to the two neutral colors in SU(3). The six remaining, charged gluons are treated as particles. We deal with these simplifications in order to be able to carry out a molecular dynamical calculation of about 400 quarks in an acceptable time. The essential confinement mechanism in this model is hidden in the scalar field self-interaction potential and the construction of the chromodielectric constant, whose particular dependence on the effective scalar field σ includes the main quantum-mechanical effect from QCD.

We think that such microscopical studies may reveal whether or not the hadronization process is faster than the maintenance of thermal or chemical equilibrium, whether or not the formed hadrons are close to the predictions of constituent quark models, and what kind of color-neutral clusters form in abundance. We think that the drawbacks of this approach, namely, the classical treatment of the color charge and its clusters, the Abelian dominance assumption in the long-range fields, and the use of the σ field, are outweighted by the advantages: an event-by-event, microscopic, dynamical simulation including flux tubes that are nonelementary but formed by a dynamical process. This is useful for studies of possible hadronization scenarios of quark matter until real-time QCD calculations become feasible.

This paper is organized as follows: in Sec. II, a brief description of the original chromodielectric model is followed by an explanation of the confinement mechanism in this model. Section III presents our practical approach to the model: we deal with the treatment of color charges in the classical limit, present our notion of hadrons within the model, and touch upon relevant computational methods. In particular, the principles of a fast adaptive multigrid finite element procedure for the solution of the Gauss law are discussed. Section IV reports on our choice of model parameters and its consequences on statical model properties. Section V is the main part of the present article: it presents actual simulation runs of hadronization scenarios. We describe our choice of initial states and show snapshots of the program runs. We then compile our results on cluster formation, and show mass, rapidity, and transverse momentum distributions for white clusters. Finally, Sec. VI summarizes our conclusions.

II. CHROMODIELECTRIC MODEL

Since free quarks have never been observed experimentally, it is generally accepted that any physical state of finite energy has to be a singlet under color-SU(3) transformations. This phenomenon is called color confinement. Since we know that classical (''tree-level'') chromodynamics does not enforce color confinement, this has to be a quantum (''loop'') effect, characteristic of a strongly interacting non-Abelian gauge field theory. However, a proof of color confinement based solely on the QCD Lagrangian has not yet been given, mainly because it is too difficult to identify the relevant QCD degrees of freedom.

The chromodielectric model tries to mimic QCD's color confinement *on the classical level* [18]. It introduces an additional scalar field σ that enforces color confinement in a conceivable way.

A. Model Lagrangian

The Lagrangian reads

$$\mathcal{L}=\mathcal{L}_p+\mathcal{L}_c+\mathcal{L}_\sigma, \tag{2.1}$$

with

$$\mathcal{L}_p=\sum_f \bar{q}^f(i\not{D}-m_f)q^f, \tag{2.2}$$

$$\mathcal{L}_c=-\frac{\kappa(\sigma)}{4}F^a_{\mu\nu}F^{\mu\nu a}, \tag{2.3}$$

$$\mathcal{L}_\sigma=\frac{1}{2}(\partial_\mu\sigma)(\partial^\mu\sigma)-U(\sigma). \tag{2.4}$$

The symbol q^f denotes a quark spinor of flavor f; both the color and Dirac indices are suppressed, and the Feynman dagger notation $\not{D}=\gamma^\mu D_\mu$ is used. The covariant derivative $iD_\mu=i\partial_\mu-g_v A_\mu$ contains the color vector potential $A_\mu=A^a_\mu(\lambda^a/2)$, where the λ^a denote the eight Gell-Mann matrices. The color field tensor is defined as

$$F_{\mu\nu}=F^a_{\mu\nu}\frac{\lambda^a}{2}:=\frac{i}{g_v}[D_\mu,D_\nu]. \tag{2.5}$$

It obeys the classical chromodynamical field equation in a covariant medium with dielectric function $\kappa(\sigma)$,

$$[D_\mu,\kappa(\sigma)F^{\mu\nu}]=j^\nu, \tag{2.6}$$

with color current

$$j^\nu=g_v\sum_f \bar{q}^f\gamma^\nu\lambda^a q^f\frac{\lambda^a}{2}=:j^{\nu a}\frac{\lambda^a}{2}. \tag{2.7}$$

The quark field obeys a Dirac equation

$$(i\not{D}-m_f)q^f=0, \tag{2.8}$$

with a constituent quark mass m_f. The quarks can in principle be treated quantum mechanically here, while the color and σ fields are regarded as classical fields.

The scalar field σ obeys a Klein-Gordon equation with a fourth-order polynomial self-interaction $U(\sigma)$ and a complicated source term

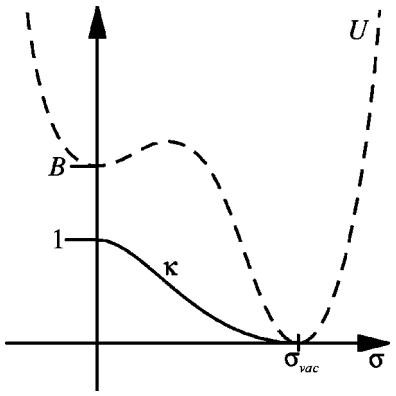

FIG. 1. Schematical graph of the functions $U(\sigma)$ and $\kappa(\sigma)$. Note that U is an energy density while κ is dimensionless. $\sigma_{\rm vac}$ denotes the value of the σ field in the physical vacuum (ground state).

$$\partial_\mu \partial^\mu \sigma + U'(\sigma) = -\frac{\kappa'(\sigma)}{4} F^a_{\mu\nu} F^{\mu\nu a}. \tag{2.9}$$

Both functions U and κ are drawn schematically in Fig. 1. Note that there is no direct coupling between the quarks and the σ field in this model.

B. Confinement mechanism

The Lagrangian (2.1) describes a classical field theory with an explicit color confinement mechanism. The ingredients of this mechanism are the self-interaction term $U(\sigma)$, the dielectric function $\kappa(\sigma)$, and the color Gauss law. In this section, we utilize a simple example to explain how these three ingredients work together to enforce color confinement.

First note that in the vacuum of this theory, $\sigma \equiv \sigma_{\rm vac}$ holds everywhere and thus $\kappa \equiv 0$. Now consider the static and color neutral quark-antiquark configuration depicted in Fig. 2. The charge distribution is given by $j_0(x) = j_0^3(x)\lambda^3/2$; i.e., it belongs to a U(1) subgroup of SU(3). The Gauss law reads, for this case,

$$\vec{\nabla} \cdot \vec{D}^3 = j_0^3. \tag{2.10}$$

It forces a color flux $\vec{D}^3 = \kappa(\sigma)(-\vec{\nabla} A_0^3 - \partial_t \vec{A}^3)$ to stretch from the quark to the antiquark. This flux cannot exist in regions where $\kappa = 0$; therefore the σ field has to deviate from its vacuum value, forming a tube (or bag) with $\sigma < \sigma_{\rm vac}$ for the flux. Assuming U and κ are defined so that σ ends up being zero in the bag, the bag formation process costs an energy density B, which in turn can be interpreted as the vacuum pressure exerted on the bag.

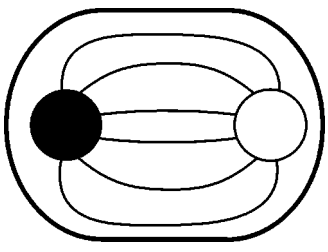

FIG. 2. A color flux tube.

Formulated differently, the vacuum pressure generated by $U(\sigma)$ and the coupling term κF^2 confines the color flux to a string—*U and κ together generate the color flux confinement*. On the other hand, the quarks cannot escape from this string because *the Gauss law demands a contiguous color flux to connect them.* Unless pair creation is allowed for, the resulting string can become arbitrarily long, causing the $q\bar{q}$ potential to rise linearly.

Let us contrast this with the corresponding result in classical chromodynamics. The Gauss law, reduced to the Abelian subgroup of our problem, reads then

$$\vec{\nabla} \cdot \vec{E}^3 = j_0^3. \tag{2.11}$$

The solution is—like in electrodynamics—simply the linear superposition of the Coulomb fields of the two charges. Since the long-distance Coulomb potential is $\propto 1/r$ and not linear, we see that classical chromodynamics does indeed not include color confinement.

III. TREATMENT OF COLOR CHARGES, FIELD EQUATIONS, AND HADRONS

A. Classical molecular dynamics approach for the charges

On our way to build a computer simulation of the CDM, we have to make several approximations. In doing so, we take care to preserve color confinement, since this is what we want to simulate.

We treat only the two commuting gluon fields $A_\mu^3 \lambda^3/2$ and $A_\mu^8 \lambda^8/2$ as classical fields; they correspond to two decoupled, color neutral fields which behave just like Maxwell fields. So from now on, the color index a is generally restricted to the values 3 and 8. This approach amounts to taking a U(1) $\times$ U(1) Abelian subgroup of the full SU(3) gauge group of QCD, and is therefore called the *Abelian approximation* [27,25]. However, in contrast to the cited works, we do not simply drop the other, charged gluons. Instead, they are treated like the quarks and antiquarks: as classical charge distributions with a Gaussian shape of fixed width. Spin and isospin are accounted for by appropriate degeneracy factors. This changes the particle Lagrangian (2.2) into the classical expression

$$\mathcal{L}_p^{\rm class} = -\sum_i \rho_N(\vec{x} - \vec{x}_i) m_i \sqrt{1 - \dot{\vec{x}}_i^2} - j^{\mu a} A_\mu^a, \tag{3.1}$$

with the color current

$$j^{\mu a} = g_v \sum_i \rho_N(\vec{x} - \vec{x}_i) q_i^a \begin{pmatrix} 1 \\ \dot{\vec{x}}_i \end{pmatrix}. \tag{3.2}$$

The index i runs over all quarks, antiquarks, and charged gluons in the system.

For the quarks, the color charges $q_i^{3,8}$ in Eq. (3.2) are equal to the diagonal entries in $\lambda^{3,8}$. Antiquarks carry the charge $-q_i^{3,8}$, and the gluons carry each the sum of one quark and one antiquark color charge. Table I and Fig. 3 summarize the possible values.

The masses m_i are model parameters; our particular choices for them are listed and explained in Sec. IV A. The

TABLE I. Quark and gluon color charges in the Abelian approximation. The color names are chosen arbitrarily but consistently throughout this article. The color shortcuts are the ones used in Fig. 3.

Particle	Color name	q^3	q^8
q	red r	1	$1/\sqrt{3}$
q	green g	-1	$1/\sqrt{3}$
q	blue b	0	$-2/\sqrt{3}$
$\bar{q}$	antired $\bar{r}$	-1	$-1/\sqrt{3}$
$\bar{q}$	antigreen $\bar{g}$	1	$-1/\sqrt{3}$
$\bar{q}$	antiblue $\bar{b}$	0	$2/\sqrt{3}$
g	red-antigreen $r\bar{g}$	2	0
g	red-antiblue $r\bar{b}$	1	$\sqrt{3}$
g	green-antiblue $g\bar{b}$	-1	$\sqrt{3}$
g	green-antired $g\bar{r}$	-2	0
g	blue-antired $b\bar{r}$	-1	$\sqrt{3}$
g	blue-antigreen $b\bar{g}$	1	$\sqrt{3}$

function ρ_N is a Gaussian number density distribution of unit norm and rms radius $\langle \vec{x}^2 \rangle = 3r_0^2$,

$$\rho_N(\vec{x}-\vec{x}_i) = \left(\frac{1}{2\pi r_0^2}\right)^{3/2} e^{-(\vec{x}-\vec{x}_i)^2/2r_0^2}. \tag{3.3}$$

In the present version of our model, particle production or annihilation is not yet included. In principle, it is no essential problem to implement them, once an appropriate probability density is at hand. This remains for future work.

B. Hadrons as irreducible white clusters

If a quark-gluon plasma is formed in an ultrarelativistic heavy-ion collision, the droplet as a whole has to be a color-SU(3) singlet. Since our numerical model respects only an Abelian U(1)×U(1) subgroup of the SU(3) symmetry group, an ''SU(3) color singlet'' is represented simply by a ''white'' cluster, i.e., one that is color neutral with respect to both the λ^3 and the λ^8 charge (cf. Fig. 3). An SU(3) color singlet is then built ''automatically'' by the presence of classical A_μ^3 and A_μ^8 fields, as solutions of Eq. (2.6). Our simulation therefore starts off from a large but white quark-gluon plasma droplet.

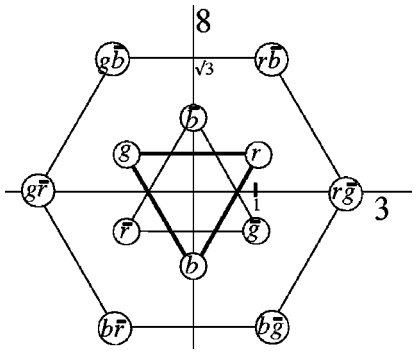

FIG. 3. Quark and gluon colors. The bold equilateral triangle corresponds to the quark colors, the other triangle to the antiquark colors, and the regular hexagon to the six charged gluons. The denotations r, g, b, $\bar{r}$, $\bar{g}$, $\bar{b}$ are chosen arbitrarily.

In nature, the hadronization process then divides the initial large cluster into a number of hadrons that are themselves separate color singlets. Correspondingly, our simulation is supposed to end up in a final state of small, white clusters that can be interpreted as hadrons. In this section, we investigate and classify the sorts of small clusters that we expect to find in the final state.

Imagine a small, white cluster of color charges. Suppose it cannot be subdivided into smaller but still white subclusters. Then, flux tubes bind the cluster together, forcing it to rotate or oscillate in a ''yoyo'' mode [25,26]. Thus it will emit σ waves, which cool the cluster down. Finally, all the color charges are resting with respect to each other, being centered at the same point in space. If we choose the same color charge distribution width for all particle species, the final cluster's charge density will vanish identically; therefore, all fields will take on their repective vacuum values in this cluster.

Because of the vanishing of all fields, two such clusters that happen to be close to each other can neither attract nor repel, and a small relative momentum suffices to separate them spatially. Consequently, we may conclude that *the final state of our simulation must be a collection of irreducible white clusters*, i.e., white clusters that cannot be divided into white subclusters. It turns out that only a finite number of possible color combinations can form irreducible clusters, which enables us to classify them, according to Fig. 4, as mesonic, baryonic, and pure glueball states. The latter occur as mesonic resonance states in the experimental observation.

We can turn this argument around, asking what clusters of quarks and gluons in our model correspond to hadrons. A hadron is supposed to be white but strongly bound. This leads us again to the notion of an irreducible white cluster. If the hadron is in its ground state, the colored constituents are all lying on top of each other, creating a local color charge density that is vanishing everywhere. Consequently, a cold hadron in our model is completely field free, and its mass equals simply the sum of the masses of the constituents, without any interaction contribution. E.g., look at the (qqq) baryon displayed in Fig. 4. The three quarks carry the colors red, green, and blue, in the meaning of Fig. 3. This baryon is certainly white, and it is also strongly bound: if one of the quarks, say, the blue one ($q^3=0$, $q^8=-2/\sqrt{3}$), tried to escape, a flux tube of a strong D^8 field would build up, pulling the fragments together with a force of 1 GeV/fm. In the ground state, the three color charges sit right on top of each other, creating a locally vanishing color charge density. In this case, all fields take on their respective vacuum values, and the cold baryon possesses a mass $3m_q$, where m_q is the quark mass.

When studying hadronization processes, our program checks at each time step whether there are irreducible white clusters in the system. A ''cluster'' in the computational sense is a set of color charges located in a common σ field bag (defined here as a connected spatial domain with $\kappa > \frac{1}{2}$). The bag vanishes for cold clusters in our model (see Sec. III B); so if a set of charges is outside any σ field bag but very close in phase space, we treat it as a cluster as well.

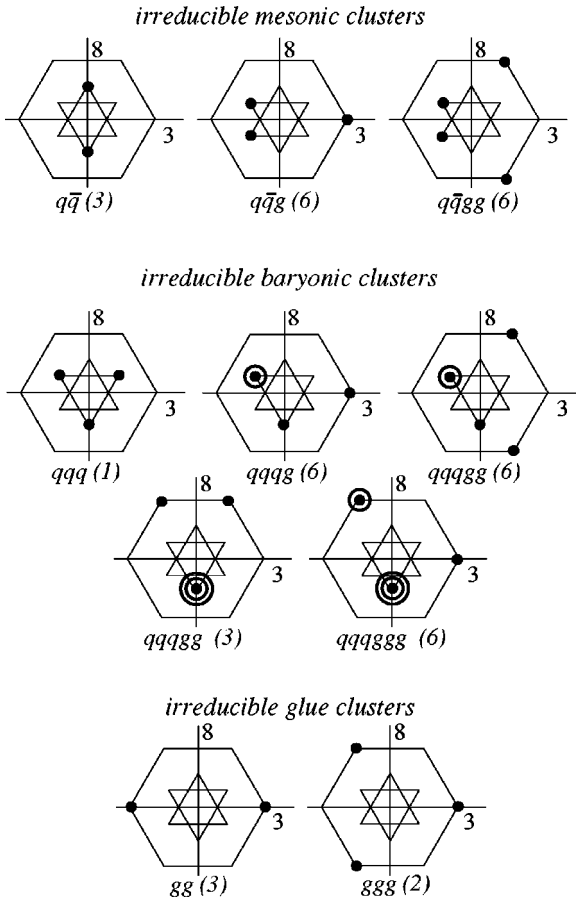

FIG. 4. Classification of irreducible white clusters in the color diagram of Fig. 3. Points and circles indicate the occupation number of each color state. Numbers in brackets indicate the color degeneracy of the diagram for each quark flavor combination.

If the cluster is irreducibly white, i.e., possesses one of the color structures displayed in Fig. 4, it is considered to be a new hadron. The program then classifies the hadron according to its color structure, computes particle and field contributions to momentum and energy, removes the charges and field imprints from the simulation as well as possible, and generates a hadron, i.e., a white, noninteracting object that just proceeds on a straight path and may even leave the lattice.

Regarding the hadrons as noninteracting neglects only color dipoles and higher multipoles, which cannot interact remotely through the model vacuum ($\kappa=0$). A description of long-range hadron-hadron interactions, which are weak anyway in comparison to the strong confinement forces, is thus beyond the scope of this simulation.

A short side remark is in order: In the investigation of the chromodielectric model, many authors (including the original inventors of the model) added a term

$$\mathcal{L}_{p\sigma}=-\sum_f \bar{q}^f g_S \sigma q^f \tag{3.4}$$

in the Lagrangian, coupling the scalar quark density directly to the σ field. This generates a high constituent quark mass outside a bag, which causes a high-density phase transition to occur in the constant field approximation (see, e.g., [28,29]). The coupling term also establishes bound solitonic states [18,23,24,30] with vanishing color charge density. Here we do not include the term (3.4) in the Lagrangian (2.1). If we did, the irreducible, final clusters of a simulation run would not be field free but rather generate a local dip in the σ field. This would generate a short-range attractive force between the white clusters: they would forever stick together, cool down by the emission of σ waves, and end up as a single large and cold object, spoiling the hadronization process we want to model.

In the model flavor presented here, there is neither an attractive nor repulsive classical force between cold (field-free) hadrons. It is interesting to note in this context that Koepf *et al.* [31] have found a soft and short-ranged *NN*-repulsive potential in a quantum-mechanical investigation within certain approximations of the very same model.

C. Numerical solution of the field equations

Let us recall the equations of motion obtained from the Lagrangian (2.1) with the classical particle term (3.1). The quarks and charged gluons feel a Lorentz force coming from the color field,

$$m_i \frac{d^2\vec{x}_i}{dt^2}=q_i^a\left(\vec{E}^a+\frac{d\vec{x}_i}{dt}\times\vec{B}^a\right). \tag{3.5}$$

The σ field equation, rewritten from Eq. (2.9), reads

$$\frac{\partial^2\sigma}{\partial t^2}=\nabla^2\sigma-U'(\sigma)-\frac{\kappa'(\sigma)}{4}[(\vec{E}^a)^2-(\vec{B}^a)^2]. \tag{3.6}$$

The σ field is stored on a 125^3-sized lattice with a volume of $(25\ \text{fm})^3$, and both the particle and σ field equations of motion are solved by a simple explicit time step method (staggered leapfrog, step length 0.04 fm).

The color fields obey the classical Maxwell equations

$$\vec{\nabla}\cdot[\kappa(\sigma)\vec{E}^a]=\rho^a, \tag{3.7}$$

$$\vec{\nabla}\times\vec{E}^a=-\frac{\partial\vec{B}^a}{\partial t}, \tag{3.8}$$

$$\vec{\nabla}\cdot\vec{B}=0, \tag{3.9}$$

$$\vec{\nabla}\times[\kappa(\sigma)\vec{B}]=\vec{j}^a+\frac{\partial\kappa(\sigma)\vec{E}^a}{\partial t}, \tag{3.10}$$

with charge and current densities given by Eq. (3.2). These equations cannot be treated by an explicit time step method. The reason is that the Gauss law (3.7), being a constraint equation, contains no time derivative and therefore constitutes an implicit condition that has to be satisfied at each time step separately.

To simplify the problem, we neglect the $\vec{B}^{3,8}$ fields in our simulation (and thereby neglect the corresponding color waves). Although breaking Lorentz invariance, it is not as bad an approximation as it may seem: it is exact for static charge configurations like in the computation of the string tension (Fig. 5); it is also exact for ''yoyolike'' excitation

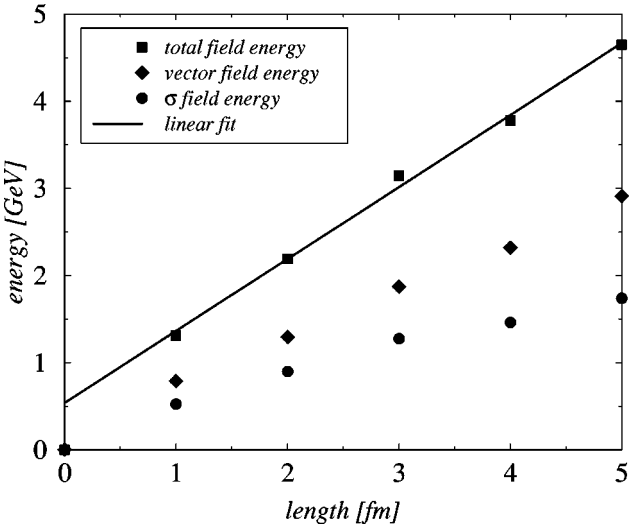

FIG. 5. The $q\bar{q}$-flux tube energy (σ and color field contributions) plotted against the separation distance of the quarks. The slope is about 1 GeV/fm.

modes of flux tubes in their rest frame [32]. Furthermore, the color confinement mechanism explained in Sec. II B is not broken by this approximation. Finally, the color field waves cannot mediate forces or transfer energy between hadronic bags because the Poynting vector $\kappa\vec{E}\times\vec{B}$ vanishes anyway in the physical vacuum. So neglect of $\vec{B}$ amounts to a neglect of some inner degrees of freedom of clusters that are nonessential for the confinement transition.

Neglecting $\vec{B}^a$, it is clear from Eq. (3.8) that $\vec{E}^a$ can now be derived from a single potential,

$$\vec{E}^a = -\vec{\nabla}\phi^a. \tag{3.11}$$

The Gauss law (3.7), rewritten in terms of ϕ^a, reads

$$\nabla\cdot[\kappa(\sigma)\nabla\phi^a] = -\rho^a. \tag{3.12}$$

This is still a constraint equation, modeling the constraint of quark confinement. It constitutes a boundary value problem that has to be solved at each time step of the simulation. This has to be done carefully since the color electric flux is an essential ingredient of the confinement mechanism.

Note that Eq. (3.12) is singular in regions where κ vanishes; this is a major obstacle to numerical treatment. We overcome it in practice by choosing a nonzero but small value for $\kappa_{\rm vac}$ (see Sec. IV A). Still, Eq. (3.12) is nearly singular and correspondingly difficult to solve. A well-tuned successive overrelaxation scheme (SOR) on a fixed grid with N^3 points, possessing at the very best a time complexity of $\mathcal{O}(N^4)$ [33], does not suffice here. Fourier transformation methods are excluded because of the nonconstant coefficient function $\kappa(\sigma)$. So we choose a fast solution algorithm based on the hierarchical basis multigrid method [34]. We are using a tetrahedral mesh of finite elements and take piecewise quadratic basis functions for the Ritz-Galerkin variational ansatz. During the multigrid iterations, the mesh is adaptively refined by bisection [35], which leads to block-diagonal matrices on each level of the multigrid scheme [36]. Refinement is performed only in those regions where the solution function varies with short wavelengths, e.g., close to the charges. This guarantees a certain precision of the solution ϕ^a independently of the structure of the sources ρ^a or the coefficient function $\kappa(\sigma)$.

There is a problem related to image charges. Imposing Dirichletian boundary conditions on the boundary surface of our cubic domain, any color charge that comes close to the boundary ''sees'' an image charge reflected at the boundary surface. In fact, even flux tubes between a charge and its image charge can be created, which yields a particularly spectacular picture if a single color charge is put in the model world. Image charges, however, are unphysical because the domain boundary is unphysical—real-world space is infinite. Fortunately, there is a simple trick to remove image charges: we make the cubic domain of the ϕ^a field much larger—$(40\ \text{fm})^3$—than the $(25\ \text{fm})^3$ lattice of the σ field. Since no color charge can leave the inner lattice (it would go into a region where $\sigma=\sigma_{\rm vac}$), it will never get close enough to the domain boundary to feel forces from its image charge. The adaptive mesh refinement method allows us to enlarge the computational domain like this (a factor of 5 in its volume) without an even noticeable increase of computing time.

Typical meshes resulting from the refinement process contain about 10^4–10^5 simplexes (tetrahedra) on about 20 levels. The Ritz-Galerkin ansatz decays on the various levels into about 10^4 small linear systems of equations, each linear system involving about 40 nodal field values. This huge data structure has to be rebuilt from scratch at each time step, since $\kappa(\sigma)$ is changing. To save computing time, caching of matrices and lazy evaluation techniques prove to be extremely useful.

The whole process of solving the Gauss law takes about 30 steps, in which adaptive refinement alternates with relaxation (solution) of the underlying equation. In each such relaxation run, the hierarchical multigrid method relaxes the Ritz-Galerkin equations in some 10–30 V-cycle iterations; their convergence is further accelerated by an Aitken transformation method applied to all nodes.

The CPU time thus needed for one solution of Eq. (3.12) varies between 15 and 200 s on a Pentium Pro 200 MHz machine, depending mainly on the structure of the source function ρ^a and κ, which in turn depend mainly on the number of charges present.

The quality of the solution is such that we never observe free color charges in actual simulation runs, and even the interaction between larger clusters that carry nonzero total color is strong enough that they do not separate.

IV. STATICAL MODEL PROPERTIES

Before studying dynamical properties, like the time evolution of a quark-gluon plasma, in the present model, let us briefly discuss our choice of model parameters, which is based solely on certain desired time-independent observables, namely, the hadronic mass spectrum, and color flux tube properties.

A. Choice of model parameters

We choose the same charge distribution radius $\sqrt{\langle\vec{x}^2\rangle} = 0.7$ fm for all the various particle flavors. The model pos-

TABLE II. Quark and gluon effective masses, and corresponding hadron masses (particle data table). All masses are measured in MeV. The symbol q denotes an up or down quark, s a strange quark, and g a gluon.

Particle	Model mass	Expt. mass	Error
q	400		
s	550		
g	700		
$\frac{1}{2}(N+\Delta)(qqq)$	1200	1086	+10.5%
$Y(qqs)$	1350	1385	−2.5%
$\Xi(qss)$	1500	1530	−2.0%
$\Omega(sss)$	1650	1672	−1.3%
$\rho(q\bar{q})$	800	770	+3.9%
$\omega(q\bar{q})$	800	782	+2.3%
$K^*(q\bar{s})$	950	892	+6.5%
$\Phi(s\bar{s})$	1100	1020	+7.8%
gg	1400	1400?1	

sesses in this case a particularly simple ''hadron spectrum.'' Cold (unexcited) hadrons are white (color-neutral) combinations of several particles centered at the same location. Their color charge distribution vanishes everywhere; therefore the fields all take on their vacuum values. Thus, the mass of such a hadron is simply the sum of the masses of its constituents. In order to obtain roughly the proper hadronic mass scales, we have chosen a nonstrange quark mass of 400 MeV, yielding a mass of 800 MeV for the ρ meson and 1200 MeV for the nucleon. The other masses are all given in Table II. This table exhibits a reasonable agreement between model and experimental numbers; fine-tuning could certainly improve this even further.

The parameters of the quartic potential $U(\sigma)$ and the dielectric function $\kappa(\sigma)$ are harder to fix since there is no well-known physical particle associated with σ. However, if we interpret σ waves as pure glueballs with a mass of about 1400 MeV, we obtain $U''(\sigma_{\rm vac})=(1400\ {\rm MeV})^2$. Furthermore, the bag constant $B=(150\ {\rm MeV})^4$ and $\sigma_{\rm vac}=0.31\ {\rm fm}^{-1}$ are chosen in order to get a low bag surface tension—which is easier to handle numerically—while still having a region with $U''(\sigma)<0$, which is a necessary condition for a first-order color deconfinement phase transition to occur. Our particular choices are motivated by studies of solitonic states in the model [23,24]. Finally, we use

$$U(\sigma)=B+a\sigma^2+b\sigma^3+c\sigma^4, \tag{4.1}$$

with $a=6.184\ {\rm fm}^{-2}$, $b=-80.72\ {\rm fm}^{-1}$, $c=163.1$, and $B=(150\ {\rm MeV})^4$. For κ, it turns out that the simulation results are not very sensitive to its precise shape. As described in the last section, its only purpose is to couple the vacuum pressure generated by $U(\sigma)$ to the color flux tube. For doing this, the κ function has to take on a value much smaller than 1 near $\sigma\approx\sigma_{\rm vac}$. Second, κ has to rise quickly to 1 where $U(\sigma)\approx B$, supporting our interpretation of B as a bag constant. We use

$$\kappa(\sigma)=\frac{1}{\exp[\alpha(\sigma/\sigma_{\rm vac}-\beta)]+1}, \tag{4.2}$$

with $\alpha=5$ and $\beta=0.4$.

Finally, the strong coupling constant $\alpha_S=g_v^2/4\pi$ is chosen such that the $q\bar{q}$ string tension equals about 1 GeV/fm, a value that can be deduced from quarkonium spectroscopy [37]. Anticipating the results of the next section, we show in Fig. 5 that a value of $\alpha_S=2$ results in a satisfactory numerical string tension.

B. Statical properties of flux tubes

Of course, the string tension, plotted in Fig. 5 and already discussed in the last section, is the flux tube property most relevant to the hadronization process. Also, all our model parameters are already fixed by the considerations done in the last section. Nevertheless, we would like to show pictures of color flux tubes and their fields. We do this in Fig. 6: Figure 6(a) shows the color flux $\vec{D}^8=-\kappa(\sigma)\nabla\phi^8$ between a blue quark and an antiblue antiquark (in the nomenclature of Fig. 3). The vector field is displayed in a plane containing both quark centers—the computation has of course been performed in three dimensions. The spheres at both ends of the flux tube represent the quarks; their radius indicates the rms radius of the color charge distributions (0.7 fm). It can be clearly seen that the color flux is indeed nicely parallel, as would be expected from a string configuration. The string radius turns out to be rather large—about 1 fm. In terms of our irreducible white cluster classification of Fig. 4, this string is an excited meson of the $q\bar{q}$ type.

Figure 6(b) shows the σ field for the same charge configuration. The contour lines are drawn at σ values of 0, 0.1, 0.2, 0.3 (from the inside outwards), where $\sigma_{\rm vac}\approx 0.31$. Remember that the only source term of the σ field is given by $\kappa'(\sigma)F^2/4$; thus, the vector field drawn in Fig. 6(a) effects a field imprint that does not fully extend over the quarks. Now we added a direct quark-σ coupling term (3.4), taking $g_S=8$ and approximating $\bar{q}q$ by the quark number density given in Eq. (3.3). The result is Fig. 6(c), differing from Fig. 6(b) only slightly, since the quark-σ coupling affects only the end points of the flux tube.

Last, Fig. 6(d) shows the σ field for a gluonic string. The total color flux is larger here: since the gluons carry each the sum of a quark and an antiquark color, the total gluon charge $\sqrt{(q^3)^2+(q^8)^2}$ is larger by a factor of $\sqrt{3}$ in comparison with a quark charge (see Sec. III A; for this picture, we took the gluon colors $r\bar{g}$ and $g\bar{r}$). The total color flux is therefore enhanced by the same factor (enforced by the Gauss law). This results in a larger pressure of the flux lines, which dig a significantly wider ''hole'' in the nonperturbative vacuum. In terms of our irreducible cluster classification scheme of Fig. 4, this gluonic string is an excited glueball of type gg.

We can also use our program to investigate a possible string-string interaction. The σ field of parallel and antiparallel configurations of two strings is plotted in Figs. 7 and 8. For the parallel case (Fig. 7), we see no notable deformation of the strings as they approach each other, while in the antiparallel case (Fig. 8), the strings ''flip,'' since the field configuration of lowest energy (which is the static solution of the field equations) is the one that connects only the closest quarks by flux tubes.

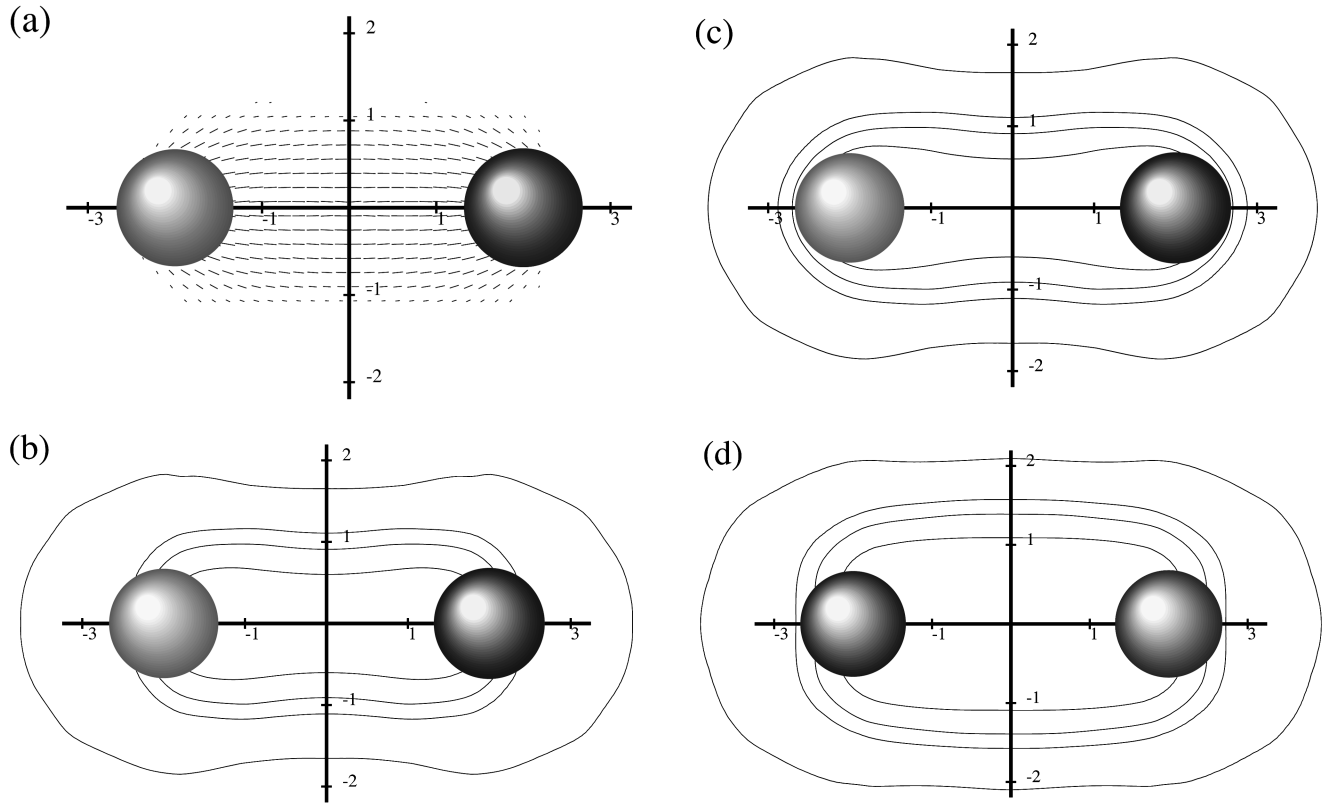

FIG. 6. (a) Vector field of a quark string of length 4 fm, (b) its σ field, (c) modification caused by an additional scalar coupling term (3.4) with $g_S=8$, and (d) σ field of a gluonic string. The contour lines are defined by $\sigma=0$, 0.1, 0.2, and 0.3 ($\sigma_{\mathrm{vac}}\approx 0.31$). Axis ticks are in units of 1 fm.

Figures 9 and 10 show the corresponding string-string potentials. For the parallel case (Fig. 9), the potential differs little from a constant, possessing a slightly attractive part (bag fusion) and a repulsive core (Coulomb repulsion). The potential of the antiparallel configuration (Fig. 10) shows the expected stringlike (linear) behavior as soon as the strings are flipped (below 4 fm).

V. HADRONIZATION OF A QUARK-GLUON PLASMA

The described simulation tool enables us to follow the microscopic dynamics of hadronization. However, in order to gain a qualitative insight, we restrict the first analysis to a few observables. In the next section, we present our choice of hadronization scenarios. Then, we introduce some important observables and explain our means of obtaining them from simulation data. Finally, we discuss our results on mass distributions and the evolution of the quark-gluon-hadron matter composition, and analyze spectral properties.

A. Initial state of the simulation

When carrying out a molecular dynamic simulation on the quark-gluon level, one has to make compromises. Even using modern computers and state-of-the-art numerical methods, we cannot simulate systems larger than a few hundred of particles in a volume of $(25\ \mathrm{fm})^3$. The entire simulation run takes finally about a 200 fm, corresponding to weeks of CPU time on a Pentium Pro 200 MHz system.

As a result of the above-mentioned restrictions we decided to simulate only a central part of the heavy-ion collision region, including about 400 quarks and gluons in an initial volume of about 100 fm^3. In real Pb+Pb collisons at CERN SPS, about 3000–4000 particles are present in the quark matter phase. We compare two different scenarios in order to gain a qualitative insight into the hadronization: (i) a fully stopped quark matter at initial temperature $T_0=160$ MeV and (ii) a hot quark-gluon plasma initialized on top of a Bjorken flow stretching from coordinate rapidity $\eta_0=-0.5$ to $\eta_0=+0.5$.

The reaction volume is calculated assuming a radius of the initial sphere of $R_0=4$ fm or of the initial cylinder of $R_0=4$ fm, respectively. The initial energy density of $\varepsilon_0=2.5\ \mathrm{GeV/fm}^3$ is obtained from the total bombarding energy characteristic for SPS. The initial numbers of quarks and gluons are chosen according to nonrelativistic Maxwell-Boltzmann statistics, using the respective masses and the initial temperature. The ratios of various flavor quarks and gluons are determined from equilibrium principles (law of mass action), being proportional to

$$N_i(0)\propto e^{-m_i/T_0} d_i \left(\frac{m_i T_0}{2\pi}\right)^{3/2}, \tag{5.1}$$

with d_i the spin, color, and flavor degeneracy. The resulting parton numbers are 133 light quarks, 40 strange quarks, the same numbers of respective antiquarks, and 44 gluons for the Bjorken event and 196 light quarks, 52 strange quarks, and 57 gluons for the full stopping event. The random Gaussian momenta (on top of the initialized flow pattern) satisfy

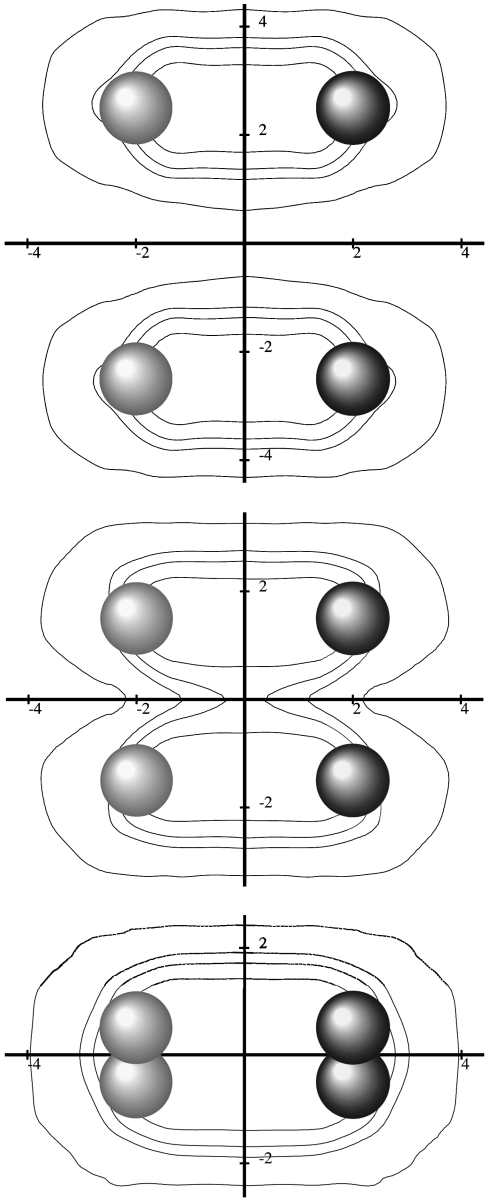

FIG. 7. Fusion of parallel flux tubes. The contour lines are at the same σ field values as in Fig. 6.

$$\left\langle \frac{p_{i,\mu}^2}{m_i} \right\rangle = T_0 \tag{5.2}$$

for each particle species and momentum components $\mu = x$, y, or z. We do not consider a nonzero quark chemical potential in the present work; furthermore, there is no net color and no net strangeness in the system.

A short side remark: a possible third scenario, a fully ''transparent'' picture where the particles are initially separated in phase space, leads to a rapid separation into unconnected parts (the spectators), leaving only a small fraction of miniclusters in the midregion. Unfortunately, we cannot simulate too large relative momenta at present, due to the computational restriction to intermediate-size simulation volumes. Some particles bounce back from the lattice boundary and interfere artificially with others still in the expanding fireball. This is unphysical, and we have to abandon our studies of this scenario at this point.

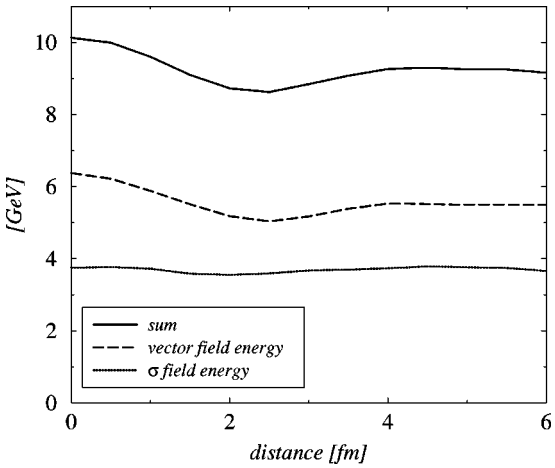

FIG. 8. String-string potential for the parallel case.

B. Identification of observables

The basis of our identification of observables is the white cluster classification and hadronization mechanism described in Sec. III B. The total momentum and total energy of white clusters can be calculated from the individual four-momenta of its constituents and from the field energy carried by the classical vector fields. The mass of a cluster is defined by

$$M_{\mathrm{clus}}^2 = \left(E_{\mathrm{field}} + \sum_i E_i \right)^2 - \left(\vec{p}_{\mathrm{field}} + \sum_i \vec{p}_i \right)^2. \tag{5.3}$$

Here,

$$E_{\mathrm{field}} = \int d^3x \left(\frac{1}{2}\dot{\sigma}^2 + \frac{1}{2}(\vec{\nabla}\sigma)^2 + U(\sigma) + \frac{1}{2}\kappa(\sigma)\vec{E}^a\vec{E}^a \right),$$

$$\vec{p}_{\mathrm{field}} = -\int d^3x \dot{\sigma}\vec{\nabla}\sigma. \tag{5.4}$$

The mass distribution dN/dM tells the number of clusters with a mass between M and $M+dM$. The resolution dM of the mass binning is chosen to be $dM = 100$ MeV presently. If dM is too large, one cannot distinguish different particles; if it is too small, the statistics become too low. The above value is a compromise found by trial and error.

Further observables are the rapidity distribution dN/dy with

$$y = \frac{1}{2}\ln\frac{E+p_z}{E-p_z} \tag{5.5}$$

and the transverse momentum distribution dN/dp_T with

$$p_T = \sqrt{p_x^2 + p_y^2}. \tag{5.6}$$

Collective flow and local temperature both affect these spectra: a strong longitudinal flow causes a plateau in the dN/dy distribution, while the slope of the transverse momentum spectra—if nearly exponential—includes both thermal and radially collective motion.

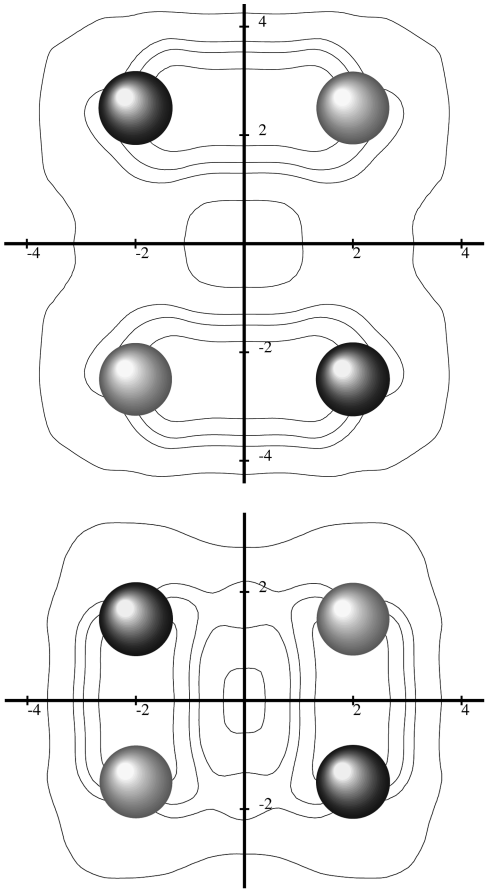

FIG. 9. Flux tubes flip in an antiparallel configuration.

Finally, some global variables are of interest in order to obtain an approximate equation of state from the molecular dynamic simulation. A temperaturelike quantity can be obtained by fitting the nonrelativistic Maxwell-Boltzmann distribution to the momenta by inspecting

$$T_{i,\mu}=\langle p_{i,\mu}^2\rangle/m_i \tag{5.7}$$

for a cluster of type i with mass m_i and momentum direction $\mu=x$, y, or z. The approximate equality of these temperaturelike parameters for different spatial directions μ reflects the isotropy of the pressure, while its equality between different sorts of clusters i the chemical and thermal equilibria.

It remains for future work to analyze the cluster size distribution with its higher moments after collecting improved statistics. This can shed some light onto the order of the hadronization transition from the viewpoint of percolation theory, as recently pointed out by Satz [38].

C. Example simulation snapshots

Figures 11 and 12 show six snapshots of the time evolution for the Bjorken and ''full stopping'' scenario.[1] The simulation times of the snapshots are written inside the frames in units of fm; the frame diagonal is of length 45 fm.

[1]MPEG movies of the actual simulation runs are retrievable by anonymous ftp from ftp:tonda.physik.uni-giessen.de/pub/cdmmovie/bjorken.mpg resp. /stopping.mpg

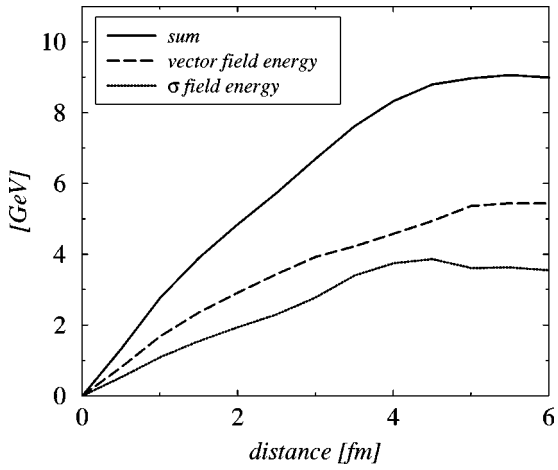

FIG. 10. String-string potential for the antiparallel case.

Quarks, gluons, and hadrons are drawn as spheres; for better visibility of the scene, the radius of a colored object is scaled down to one-third of the actual rms radius of the charge distribution (0.7 fm). Hadron radii reflect the bag volume formed by the σ field footprint of the hadronized cluster; they are scaled down to one-half of their actual size. For white clusters without any σ field bag (see Sec. III B), we draw a sphere of radius 0.35 fm. The σ field and the two color fields are not displayed. Note that in the last frame, many hadrons have already left the scene.

As can be seen from the pictures, the initial partonic fireball is expanding and hadronizing. At each time step, the equations of motion of the charges and the σ field as well as the Gauss law are solved (see Sec. III C). Whenever an irreducible white cluster is detected (by the mechanism described in Sec. III B), it is classified according to Fig. 4 as a meson, baryon, or glueball, its total energy, momentum, and mass are computed, and the partons and their field imprint are removed from the simulation and replaced by a noninteracting ''hadron,'' displayed in the snapshots as a gray sphere.

We would like to emphasize that the production of hadronic states is not artificially put in by hand: the model itself produces irreducible white clusters in the final state, and it is only up to our detection routine to classify them and take them out of the simulation. The detection routine does not drive or interfere with the process of hadron formation; it merely serves to interpret the results. Although the last snapshot still shows quarks and gluons, this is not the final state of the simulation run. In the final state of the simulation run, hadronization is indeed complete: no partonic fireball is left over.

D. Energy conservation, hadronization time, and temperature

Figure 13 shows the energy over time of the system and its parts in the Bjorken scenario, for the same event the snapshots were taken from. Figure 14 shows for the same time interval the temperature evolution of the partons in the fireball and the produced hadrons. Their temperature is found from

$$\frac{3}{2}T:=\left\langle\frac{\vec{p}^2}{2m}\right\rangle. \tag{5.8}$$

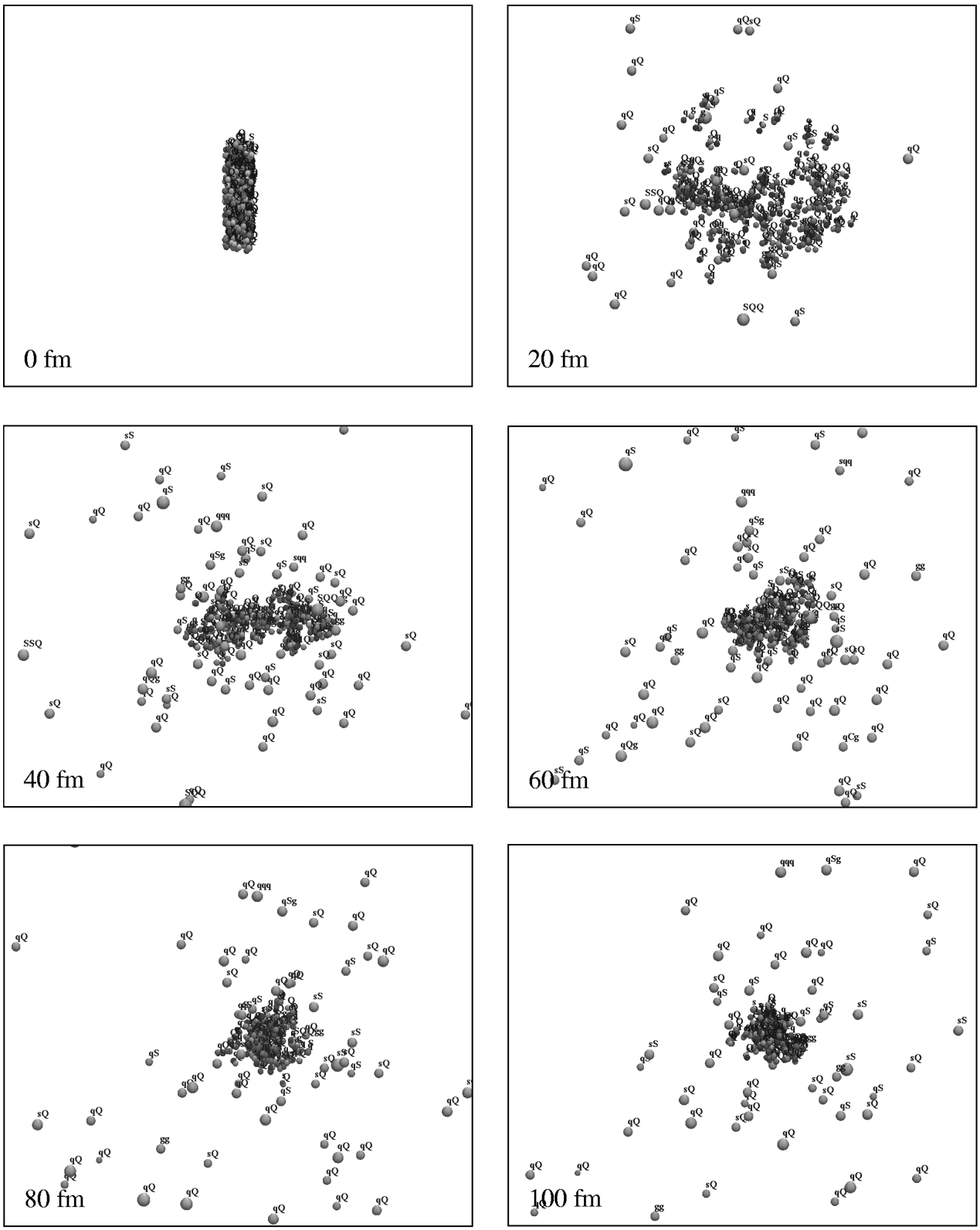

FIG. 11. Simulation snapshots after initialization of a central-rapidity slice of a QGP tube with Lorentz-invariant flow (''Bjorken scenario''). The frame diagonal is of length 45 fm. The labels at the particles and hadrons indicate the various flavors and constituents; the letter *q* represents an up or down quark; the other letters have obvious meanings, capital letters denoting antiquarks. Colored objects (quarks, gluons) are drawn in dark gray, hadrons in light gray.

The partons heat up initially because they are accelerated by relatively long (>1 fm) flux tubes. These flux tubes are present simply because of the initial spatial random distribution of the charges. Very soon, however, the hot particles cool down, transferring energy to the σ field. On the same time scale, the energy contribution of the color electric field, also shown in Fig. 13, decreases to almost zero. This is an indication of the strong electric shielding of the plasma. The

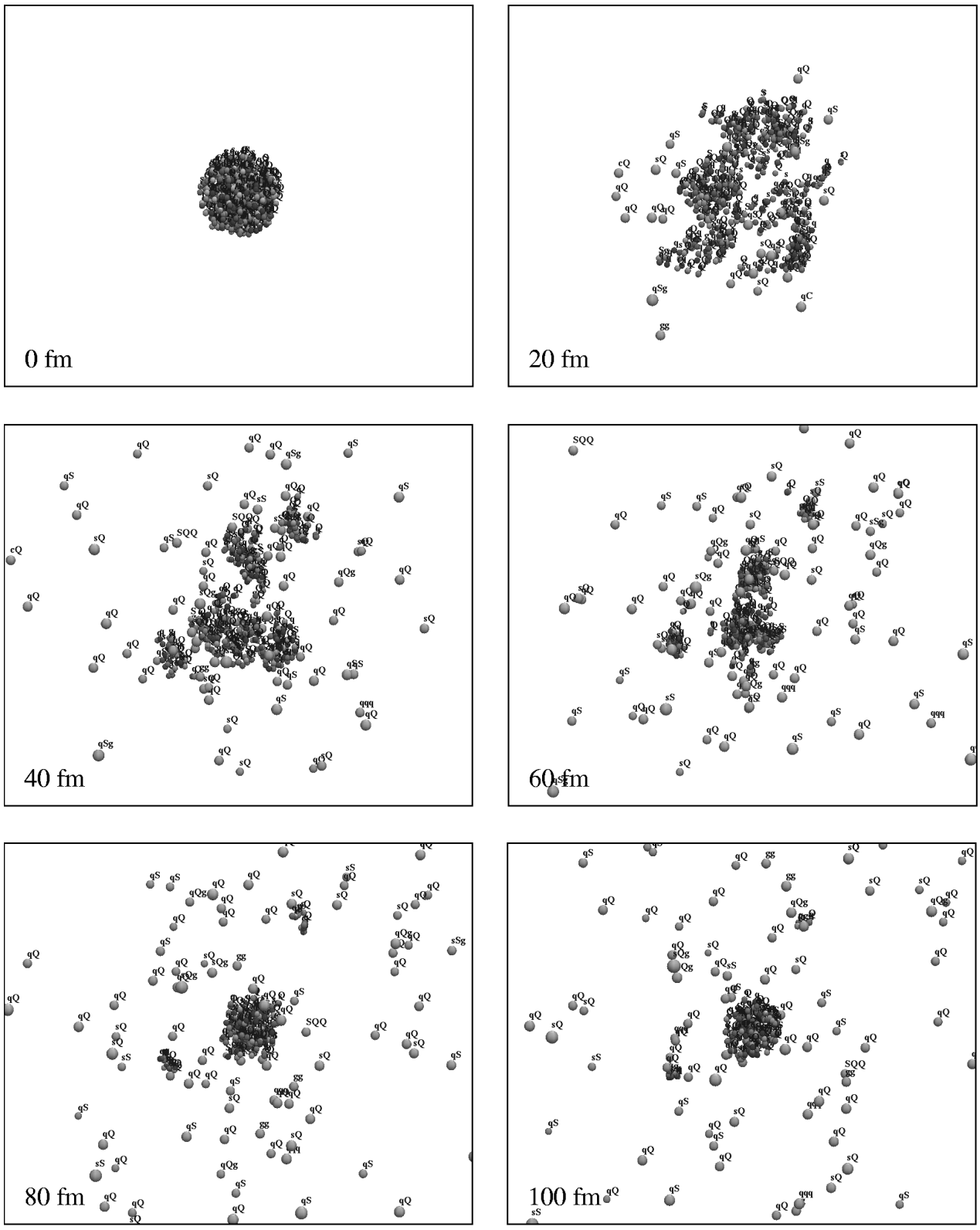

FIG. 12. Simulation snapshots after initialization of a thermal QGP fireball (''full stopping scenario'').

picture of the plasma as a collection of flux tubes breaks down here; flux tubes emerge only on the surface of the fireball, pulling back colored objects that try to escape. It is interesting to note that, although the energy contribution of the color field itself is never significant, the color field dictates the dynamics of the hadronization process, allowing only white objects to separate.

The hadronic energy contribution is a monotonous step function: it increases each time we take another quark-gluon cluster, delete its field imprint, and add it to the set of hadrons in the system. The hadrons no longer interact, hence the piecewise constant energy. About half of the final energy is deposited in σ waves. This energy has its origin in the initialized thermal energy of the color charges. These form flux

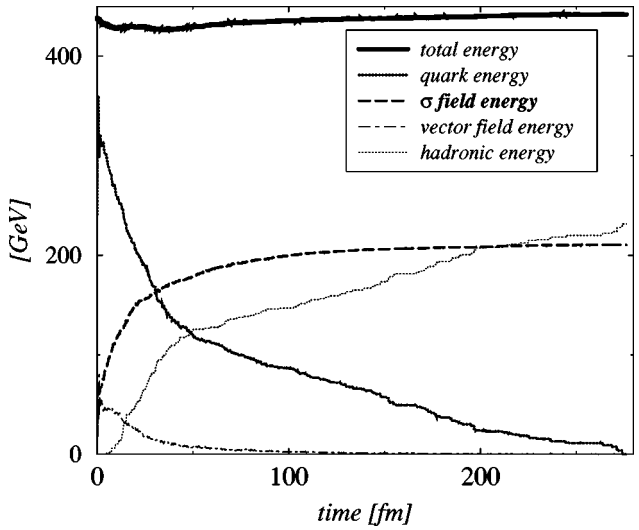

FIG. 13. System energy during time evolution in the Bjorken event.

tubes, and via the coupling term $\kappa(\sigma)F^2/4$ the flux tube cools down, radiating σ waves. The σ field describes the long-range collective effects of QCD. Its large energy content shows that the nonperturbative QCD vacuum is highly excited; in the ''real world,'' it would decay mostly into pions which so far have not been included in our simulation.

Note that most of the final hadronic energy is produced in the time interval [10 fm, 50 fm]. These 40 fm could be interpreted as the hadronization time in our model.

There is no final-state interaction among the hadrons or between hadrons and partons in the simulation; so the hadronic subsystem is not in thermal contact with the fireball. This is realistic: the hadron temperature reflects the parton temperature at the time of hadron formation (freeze-out point). Since most of the hadrons are produced in the time interval [10 fm,50 fm], the final hadronic temperature reflects the fireball temperature at that time. The fireball cools down further, which leads to the unrealistic picture that after about 50 fm, the fireball is significantly cooler than the hadrons.

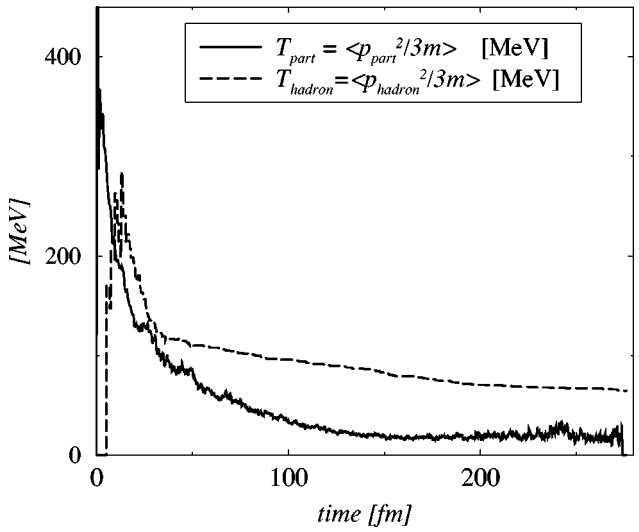

FIG. 14. Particle and hadron temperature over time in the Bjorken event.

In an experiment, a fireball as cold as 50 MeV would probably hadronize immediately. In our simulation, however, hadrons are only well defined once they have clearly left the fireball and can be *detected* as a separate, irreducible white cluster. At this late stage of the simulation run, hadronization is a random evaporation process: inside the fireball, color fields are strongly shielded, which prevents stable white clusters from forming. So an irreducible white cluster (hadron) can only form at the surface of the fireball, as soon as its constituents, floating around in the fireball nearly freely, happen to reach the surface with coalescent momenta. Thus it takes quite some time for a small, cold parton cluster to hadronize completely.

We attribute this partly to the missing repulsive interaction between the white clusters in our simulation [31]. In addition, it is well known from nuclear fragmentation studies that the mean field tends to prevent clusterization [39]. Thus, fluctuations of the color fields may be important for the final hadronization process.

E. Mass distribution

The final mass distribution of the hadrons is shown in Fig. 15 for both the Bjorken and ''full stopping'' scenarios. The spectra start at a mass of 800 MeV because this is the mass of the lightest hadron ($q\bar{q}$) in our model, and no quarks or gluons are left over in the final state.

Although the spectra do look different at first sight, one should keep in mind that since these are single events, the differences in the spectra may simply be due to statistical fluctuations and might not be significant of the respective scenario. Note also that the shape of the mass spectrum in the Bjorken case would stay the same if the chosen rapidity slice $\Delta y=[-0.5,0.5]$ were extended to a realistic interval, simply because masses are Lorentz invariant.

Assuming a Hagedorn density of hadronic states [40],

$$\rho(m)\propto m^a e^{m/T_H}, \tag{5.9}$$

we expect in the nonrelativistic limit a measured mass distribution

$$\frac{dN}{dm}\propto\rho(m)\int d^3p e^{-(m+p^2/2m)/T}\propto m^{a+3/2}e^{-m(1/T-1/T_H)}. \tag{5.10}$$

The nonrelativistic limit is justified by our large constituent masses. Here, T_H is the Hagedorn temperature: the limit temperature of hadronic strings. Beyond this temperature, the flux tube picture must be replaced by a true QGP. We assume $T_H=160$ MeV for now (which is what Hagedorn estimated originally) and take $a=-3$ from [41]. Figure 15 shows that a satisfactory fit of the form (5.10) can be obtained. Our fit parameter b is related to T via

$$b=\frac{1}{T}-\frac{1}{T_H}. \tag{5.11}$$

The corresponding hadron temperature is $T=130$ MeV for the Bjorken event ($T=146$ MeV for the full stopping event), which is somewhat higher than the kinetic temperature found in the last section. However, these numbers de-

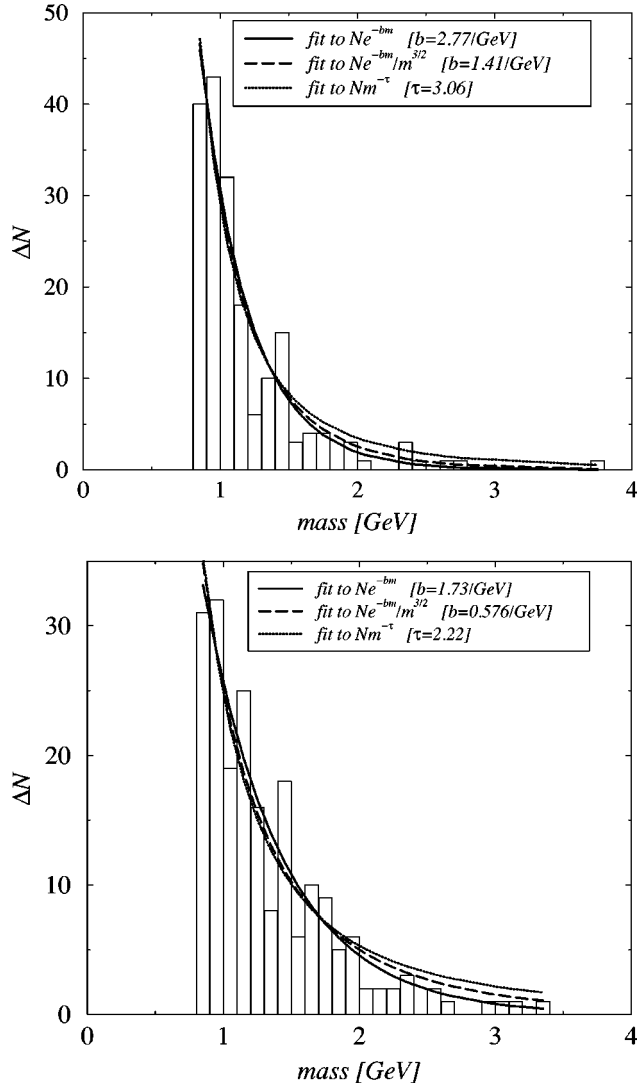

FIG. 15. Mass spectra; the upper graph is the Bjorken case, the lower the ''full stopping'' scenario.

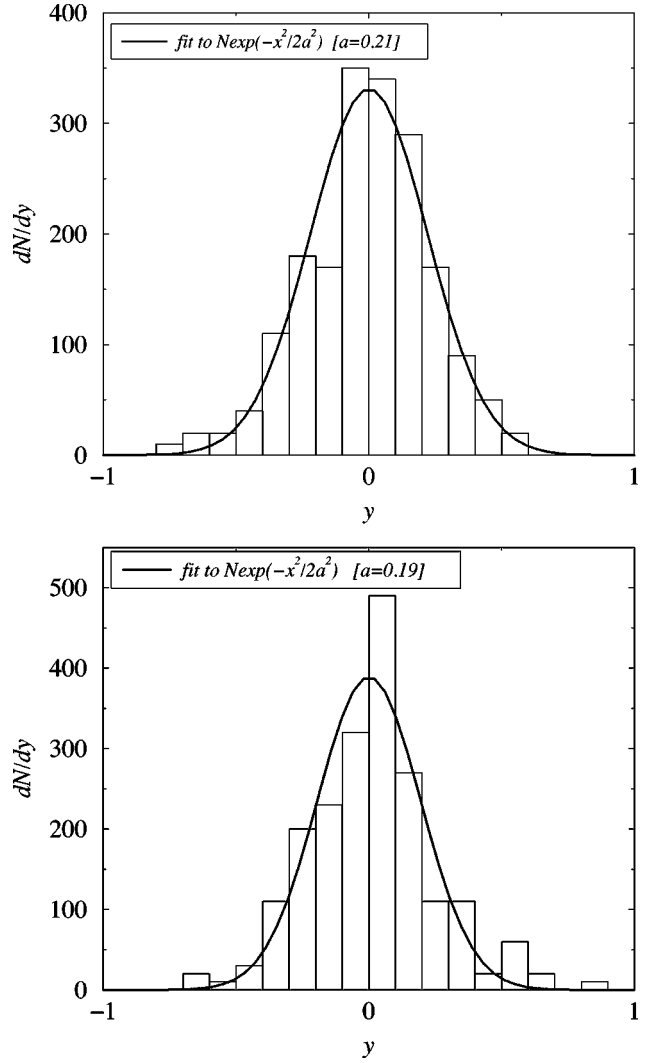

FIG. 16. Rapidity spectra; the upper graph is the Bjorken case, the lower the ''full stopping'' scenario.

pend on the choice of a: taking $a=-3/2$, we expect a simple exponential curve for the mass spectrum, which results in different values for T, namely, $T=110$ MeV for the Bjorken event and 125 MeV for the full stopping event. In this single-event analysis with our very small statistics, we cannot really decide on the correct value of a.

Another possible expectation for the mass spectrum could be that of a percolative process near the critical point [42]. There, a scaling distribution

$$\frac{dN}{dm} \propto m^{-\tau} \tag{5.12}$$

is expected. Trying to fit this relation to our data (see Fig. 15), we find a satisfactory agreement for $\tau=3.06$ (Bjorken case) and $\tau=2.22$ (full stopping event). We plan to investigate this further in the future.

F. Rapidity and momentum spectra

Figure 16 shows the hadron rapidity spectra of both scenarios. They do not look significantly different, the Bjorken

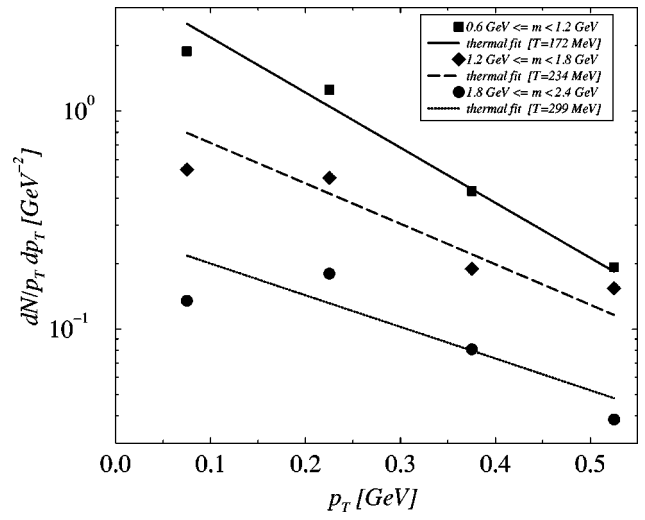

FIG. 17. Final transversal momentum spectrum for the Bjorken case, for three mass bins separately. When computing the fit lines, we took the statistical error bars correctly into account [33].

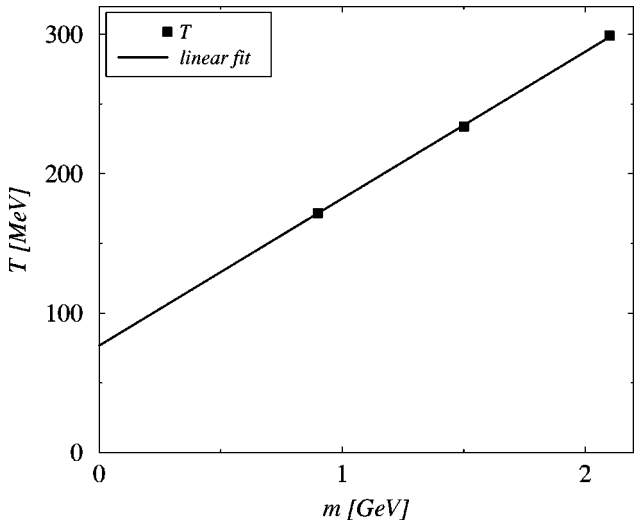

FIG. 18. The temperatures extracted from mass differential p_T spectra, plotted against hadron rest mass.

case being somewhat broader due to the longitudinal flow. However, no plateau structure is visible in the Bjorken case, since we have cut out a central-rapidity slice of the Bjorken tube. One could easily extrapolate this result by folding the rapidity spectrum with that of a Bjorken QGP tube of realistic extension. This folding process would then result in a plateau structure.

Finally, Fig. 17 shows the transverse momentum spectra of nonstrange white hadronic clusters in the Bjorken scenario, observed in mass bins of width 0.6 GeV above 0.6 GeV. Although the points in the figure representing mid-p_T values do not lie exactly on exponential curves, it is interesting to consider the slope values in order to extract possible information on the flow and temperature of the fireball in the late hadronization phase. The resulting inverse slopes, denoted as ''temperatures'' $T(m)$, are displayed in Fig. 18. By fitting to the linear relation

$$T(m) = T_0 + m\langle v_T^2 \rangle, \tag{5.13}$$

we extract from the plot a temperature $T_0 = 77$ MeV and a radial flow $\sqrt{\langle v_T^2 \rangle} = 0.32$. A direct computation of the radial flow from our final state yields $\sqrt{\langle v_T^2 \rangle} = 0.30$, which is remarkably close. For the full stopping event, the same $T(m)$ analysis yields $T_0 = 126$ MeV and $\sqrt{\langle v_T^2 \rangle} = 0.18$, while the true radial flow is $\sqrt{\langle v_T^2 \rangle} = 0.27$, a not so good agreement. Compared to data on SPS heavy-ion experiments at CERN [43] ($\langle v_T \rangle = 0.4$, $v_{\max} = 0.6$, and $T = 140$ MeV) our results display a little less flow and a colder hadronic fireball. It should be noted, however, that this analysis is based on a single event whose plasma volume is only a fraction of the experimental one. Also, we extracted the spectra of rather heavy hadronic clusters; their decay products (with lower mass) may have higher p_T slopes, leading altogether to a higher estimate of T_0. From this viewpoint, the qualitative agreement is satisfactory.

VI. CONCLUSION

We have investigated the hadronization process of a quark-gluon droplet in the framework of the chromodielectric model, using a classical molecular dynamic approach. An efficient computer code was written and put to work for the solution of the boundary value problem connected to the Gauss law in the Abelian dominance approximation. This code made it possible to study a volume of about $(25 \text{ fm})^3$, filled with about 400 particles.

Our quark masses were fitted to a constituent model of the vector meson octet and baryon decuplet states. We determined from the microscopic data of hadronization events the mass, rapidity, and transverse momentum distributions.

As example scenarios we have taken two different initial states, one with full stopping and one with a one-dimensional scaling flow. The two scenarios behave similarly, having a commensurate energy density initially. We found that although the identification of white clusters technically requires a long simulation time, the mass distribution develops a hadron part already at the beginning of the process—about 10 fm after initialization—and the main hadronization process is done after another 25 fm have passed. In a recent RQMD paper [44] similar hadronization times are reported.

Hadronization is certainly a much faster process than this simulation suggests. This is because we can only uniquely identify an irreducible white cluster after it has already left the fireball. So in this simulation, hadronization looks like a slow evaporation effect, while in principle prehadrons could already form in the plasma but remain undetected by our program. An effective, quantum-mechanical, repulsive force between white clusters, as computed by Koepf *et al.* [31], could change this picture, if a consistent way of including this in our simulation can be found.

In the present approach, hadronization is entirely due to color confinement forces, contrary to NJL-type models, where chiral symmetry determines the dynamics of hadronization [17]. These two approaches are complementary: The CDM contains perfect color confinement; its high effective quark masses must be attributed to chiral symmetry breaking. On the other hand, the NJL model contains an explicit chiral-symmetry-breaking mechanism, but no confinement. The absence of free color charges at the end of the hadronization is thus guaranteed only in the CDM.

As already discussed in Sec. V D, about half of the total energy remains in σ-field waves at the end of simulation. This points out the necessity of including pions in a possibly improved version of this model: as a result of their higher mass, the σ fluctuations would then be converted into pionic excitations. A quantitative treatment may be achieved by extending σ^2 terms to $\sigma^2 + \vec{\pi}^2$; this approach, however, would use elementary pion fields instead of light $q\bar{q}$ clusters. This is as unsatisfactory as in the NJL model. Additionally, the usual chirally symmetric extension of the σ field into a $(\sigma, \vec{\pi})$ field is inconsistent with our interpretation of σ waves as pure glue waves with a glueball mass of 1400 MeV. On the other hand, an explicit pion field would allow us to describe a long-range hadron-hadron interaction that is currently missing from our model.

We think that a more promising approach would be to treat light, relativistic quarks in the CDM. The light mesons, in particular the pion, do not fit into the string phenomenology; thus their hadronic cluster cannot be described entirely classically. The near-spherical ground states contain a large

contribution to the meson mass due to quantum uncertainty, which is negligible for effectively heavier quarks. Also, if light quarks are included, a pair production via the Schwinger mechanism will have to be considered (presently not included in the model). A quantitative treatment of these issues is beyond the scope of this article.

Summarizing, we do not observe a vast departure from thermal equilibrium during this microscopic study of hadronization. Chemical equilibration, on the other hand, is incomplete as shown by the deviation between the Maxwell-Boltzmann slopes for different cluster species and in general between colored and white particles. This also supports the conclusion that during the late hadronization of quark matter there is no phase equilibrium between the quark-gluon and hadron components; the Gibbs criteria do not apply. The suggested picture is rather a mixture of hadronic and quark-gluon plasma counterparts (with additive instead of equal pressure).

An extended study of the cluster distribution in the near future is planned in order to investigate whether the hadronization is a percolation- or phase-transition-like process.

ACKNOWLEDGMENTS

This work is part of a collaboration between the Deutsche Forschungsgemeinschaft and the Hungarian Academy of Science (project No. DFG-MTA 101/1998) and has been supported by the Hungarian National Fund for Scientific Research OTKA (project No. T019700 and T024094), and the Joint American-Hungarian Fund (JFNo. 649) as well as the Bundesministerium für Bildung, Wissenschaft, Forschung und Technologie (BMBF), and the Gesellschaft für Schwerionenforschung (GSI) Darmstadt. Discussions with C. Greiner, S. Leupold, and J. Zimányi are gratefully acknowledged.

[1] H. Satz, in *Proceedings of the Conference ''Quark Matter 91,''* Gatlinburg, TN, 1991, edited by T. C. Awes *et al.* [Nucl. Phys. **A544**, 371 (1992)].

[2] M. Creutz, *Quarks, Gluons and Lattices* (Cambridge University Press, Cambridge, England, 1983). For a recent review see C. DeTar, in *Quark-Gluon Plasma 2*, edited by R. C. Hwa (World Scientific, Singapore, 1995), p. 1.

[3] E. Braaten and R. D. Pisarski, Phys. Rev. D **42**, 2156 (1990). For a recent review see M. H. Thoma, in *Quark-Gluon Plasma 2* [2], p. 51.

[4] L. V. Keldysh, Sov. Phys. JETP **20**, 1018 (1965).

[5] Proceedings of the Workshop on ''QCD at Finite Baryon Density,'' Bielefeld, 1998; W. Bietenholz and U.-J. Wiese, Phys. Lett. B **426**, 114 (1998); S. D. Hsu and M. Schwetz, *ibid.* **432**, 203 (1998); R. Aloisio, V. Azcoiti, G. DiCarlo, A. Galante, and A. F. Grillo, Nucl. Phys. B Proc. Suppl. **63**, 442 (1998); Phys. Lett. B **435**, 175 (1998); I. M. Barbour, S. E. Morrison, E. G. Klapfish, J. B. Kogut, and M.-P. Lombardo, Nucl. Phys. B Proc. Suppl. **60A**, 220 (1998); W. Bietenholz, *Improved Lattice Action with Chemical Potential*, in Proceedings of the Workshop on ''QCD at Finite Baryon Density,'' Bielefeld, 1998 [Nucl. Phys. **A642**, 275 (1998)].

[6] B. Andersson, G. Gustafsson, G. Ingelman, and T. Sjöstrad, Phys. Rep. **97**, 33 (1983); B. Andersson, G. Gustafsson, and B. Nielssen-Almquist, Nucl. Phys. **B281**, 289 (1987).

[7] H. Fukuda and C. Iso, Prog. Theor. Phys. **60**, 1439 (1978); S. A. Azimov, G. M. Chernov, K. G. Gularnov, V. Sh. Navotnyi, and N. S. Scripnik, Phys. Lett. **73B**, 500 (1978); D. H. Boal, Phys. Rev. C **33**, 2206 (1986).

[8] R. J. Glauber, *Theory of High-Energy Hadron-Nucleus Collisions*, Methods in Subnuclear Physics, edited by M. Nikolíc, Vol. V (Gordon & Breach, New York, 1977), Pt. 1, pp. 1–52; R. J. Glauber, in *Geometrical Pictures in Hadronic Collisions*, edited by S. Y. Lo (World Scientific, Singapore, 1987), p. 83.

[9] R. P. Feynman and R. D. Field, Phys. Rev. D **15**, 2590 (1977); Nucl. Phys. **B136**, 1 (1978).

[10] K. Geiger and B. Müller, Nucl. Phys. **B369**, 600 (1992); K. Geiger, Phys. Rep. **258**, 238 (1995); J. Ellis and K. Geiger, Phys. Rev. D **52**, 1500 (1995).

[11] K. Werner, Z. Phys. C **42**, 85 (1989); Phys. Rep. **232**, 87 (1993).

[12] H. Sorge, H. Stöcker, and W. Greiner, Ann. Phys. (N.Y.) **192**, 266 (1989); M. Belkacem *et al.*, Phys. Rev. C **58**, 1727 (1998).

[13] T. S. Biró, P. Lévai, and J. Zimányi, Phys. Lett. B **347**, 6 (1995); J. Phys. G **23**, 1941 (1997).

[14] E. G. Nikonov, A. A. Shanenko, and V. D. Toneev, ''A mixed phase model and the 'softest point' effect,'' nucl-th/9802018; (private communication).

[15] H. W. Barz, B. L. Friman, J. Knoll, and H. Schulz, Nucl. Phys. **A484**, 661 (1988).

[16] T. S. Biró, P. Lévai, and J. Zimányi, ''Hadronization transchemistry from quarks to hadrons,'' hep-ph/9807303.

[17] P. Rehberg, S. P. Klevansky, and J. Hüfner, Phys. Rev. C **53**, 410 (1996); Nucl. Phys. **A608**, 356 (1996); S. P. Klevansky, P. Rehberg, A. Ogura, and J. Hüfner, ''Developing transport theory to systematically include mesons and hadronization,'' in Proceedings of the Workshop on QCD Phase Transitions, Hirschegg, 1997, edited by H. Feldmeier and J. Knoll, hep-ph/9701355, p. 397.

[18] R. Friedberg and T. D. Lee, Phys. Rev. D **15**, 1694 (1977); **16**, 1096 (1977).

[19] R. Goldflam and L. Wilets, Phys. Rev. D **25**, 1951 (1982); L. Wilets, in *Chiral Solitons*, edited by K. F. Liu (World Scientific, Singapore, 1987); G. Fái, R. J. Perry, and L. Wilets, Phys. Lett. B **208**, 1 (1988).

[20] S. Kahana and G. Ripka, Nucl. Phys. **A429**, 462 (1984).

[21] U. Mosel, *Fields, Symmetries and Quarks* (McGraw-Hill, London, 1989).

[22] U. Kalmbach, T. Vetter, T. S. Biró, and U. Mosel, Nucl. Phys. **A563**, 584 (1993).

[23] T. Vetter, T. S. Biró, and U. Mosel, Nucl. Phys. **A581**, 598 (1995).

[24] T. Vetter, Ph.D. thesis, Giessen University, 1994.

[25] S. Loh, T. S. Biró, U. Mosel, and M. H. Thoma, Phys. Lett. B **387**, 685 (1996).

[26] S. Loh, Ph.D. thesis, Giessen University, 1997.

[27] T. Elze and U. Heinz, Phys. Rep. **183**, 81 (1989).

[28] E. Naar and M. C. Birse, J. Phys. G **19**, 555 (1993).
[29] J. A. McGovern, M. C. Birse, and D. Spanos, J. Phys. G **16**, 1561 (1990).
[30] L. Wilets, *Nontopological Solitons* (World Scientific, Singapore, 1989).
[31] W. Koepf, L. Wilets, S. Pepin, and F. Stancu, Phys. Rev. C **50**, 614 (1994); W. Koepf and L. Wilets, *ibid.* **51**, 3445 (1995).
[32] L. Wilets and R. D. Puff, Phys. Rev. C **51**, 339 (1995).
[33] W. H. Press, S. A. Teukolsky, W. T. Vetterling, and B. P. Flannery, *Numerical Recipes in C*, 2nd ed. (Cambridge University Press, Cambridge, England, 1992).
[34] R. E. Bank, T. F. Dupont, and H. Yserentant, Numer. Math. **52**, 427 (1988).
[35] C. T. Traxler, Computing **59**, 115 (1997).
[36] W. Mitchell, SIAM (Soc. Ind. Appl. Math.) J. Sci. Stat. Comput. **13**, 146 (1992).
[37] D. H. Perkins, *Introduction to High Energy Physics* (Addison-Wesley, Reading, MA, 1987).
[38] H. Satz, Nucl. Phys. **A642**, 130 (1998).
[39] C. Jung, W. Cassing, and U. Mosel, Nucl. Phys. **A477**, 256 (1988).
[40] R. Hagedorn, Nuovo Cimento Suppl. **3**, 147 (1965); G. Veneziano, Nuovo Cimento A **57**, 190 (1968).
[41] M. I. Gorenstein, V. A. Miransky, V. P. Shelest, G. M. Zinovjev, and H. Satz, Nucl. Phys. **B76**, 453 (1974).
[42] D. Stauffer, Phys. Rep. **54**, 1 (1978); D. Stauffer and A. Aharony, *Introduction to Percolation Theory* (Taylor & Francis, London, 1992).
[43] NA44 Collaboration, N. Xu, Nucl. Phys. **A610**, 175c (1996).
[44] H. van Hecke, H. Sorge, and N. Xu, Phys. Rev. Lett. **81**, 5764 (1998).